Prediction of phase evolutions during Friction Stir Welding of Ti-grade 5 T-Joints using Finite Element Modeling

Davide Campanella[1, a *] and Livan Fratini[1,b]

[1]University of Palermo, viale delle Scienze, 90128 Palermo, Italy

[a, *]davide.campanella@unipa.it; [b] livan.fratini@unipa.it

Abstract. Friction Stir Welding (FSW) is a solid-state welding technology pioneered by The Welding Institute (TWI) in 1991. Originally used to weld aluminum alloys, it is now effectively utilized to weld high-resistance materials as well. Traditional fusion welding of titanium alloys provides various challenges because of the strong material reactivity with oxygen, hydrogen, and nitrogen, resulting in joint embrittlement. In this way FSW, avoiding any melting of the base material, represents a cost effective and high-quality solution. The ultimate mechanical characteristics of the joints are inextricably linked to the microstructural evolutions that occur during the process in terms of phase change. It is then crucial, in order to carry out an effective process engineering, to predict the final material microstructure determined by the thermal history occurred during the process itself. In the paper, a 3D Finite Element Method (FEM) model for the FSW of T-joints is proposed, based on a thermo-mechanical staggered analysis, able to predict the phase transition of the Ti6Al4V alloy. The model, which has been fine-tuned using experimental data, can predict the phase volume fraction in the different joint zones. The acquired findings allow to assess the effectiveness of the FSW FEM model as a process design tool.

Keywords: Friction Stir Welding; T-shaped geometry; Ti-Grade 5.

1. Introduction

During the last decades, scientists have been interested in titanium alloys because of their high strength, good corrosion resistance, and biocompatibility [1]. Titanium and its alloys have become one of the most popular light alloys in industrial applications where performance is more important than cost [2]. In fact, titanium alloys are often used as a biomedical material, even if they may have poor surface wear characteristics, limiting the performance and service life [3]. Furthermore, as surface rust worsens, microscopic particles on the surface peel off, worsening inflammation in sensitive tissues [4]. Shape memory alloys based on titanium are another field of application. Because of the difference in elastic modulus between human bones and most Ti-based shape memory alloys, such as TiNb, they offer superior shape memory effect, pseudo-elasticity, corrosion resistance, and biocompatibility [5]. Overall, adequate measures are needed to achieve control of titanium alloys' microstructure and characteristics, allowing them to better satisfy requirements in a variety of working situations.

For the above-mentioned reasons, the aircraft industry makes extensive use of these alloys, being one of the primary drivers a constant focus on lowering the weight reduction. Furthermore, a great effort has been carried out in the last decade in order to reduce the so called buy to fly ratio, reducing the machining operations to get the final desired shapes and enhancing both forging and welding operations. As far as the latter are regarded, Friction Stir Welding (FSW) has been investigated in deep in recent years because of its ability to successfully weld similar and dissimilar lightweight materials, even titanium alloys characterized by a very low value of thermal conductivity. The process mechanics, in a simple butt joint configuration, is determined by a specially developed rotating tool that is inserted with a proper tilt angle into the adjoining edges of the sheets to be welded and then moved all the way along the joint. The actual joining of the blanks occurs in solid state conditions,

the tool produces frictional and plastic deformation heating in the welding zone determining material softening and activating a proper material flow for which the solid bonding conditions in terms of temperature, pressure and time are reached. The material is pushed to flow around the tool as it goes along the welding line and rotates, creating a complex flow pattern: this effect was extensively explored for butt joints, especially as the technique was first proposed [6]. FSW has been utilized first by aeronautical engineers to weld materials that cannot be effectively welded by traditional fusion welding, such as the aluminum alloys of the 2XXX and 7XXX series [7], as well as to replace riveting [8].

A few research can be also found in literature on FSW of titanium alloys. Zhang et al. [9] investigated the mechanical and metallurgical properties of FSW joints made from commercially pure titanium sheets with thicknesses of 5.6 mm and 3 mm, determining the feasibility of the process for such materials and highlighting the main differences from the microstructure evolution phenomena seen in FSW of aluminum alloys. Pasta and Reynolds [10] used numerical simulation to study the effects of residual stress on fatigue fracture propagation in Ti-6Al-4V titanium alloy; in particular, their numerical model was focused on crack growth rate prediction and demonstrated good agreement with experimental results.

It should be observed that the geometry of the T configuration (T-joints) provides crucial properties in terms of stiffness and strength of a structure, which can be enhanced greatly without adding considerable weight [11]. FSW may be a viable solid-state joining approach for producing titanium alloy T-joints. Technological parameters such as tool rotation speed and tool feed rate must be carefully selected since they have a significant impact on the specific thermal contribution conferred to the joining edges. Furthermore, in the T-joints case the actual surface to be welded is horizontal, namely somehow parallel to the material flow induced by the rotating tool and its pin. This make more difficult to get effective solid bonding conditions in terms of pressure and a larger value of heat flux is needed. Detailed information on the impact of process parameters on the FSW process mechanics and welded joint performance can be found, for example, in a study by Liu et al. [12]. Because of the above cited complexity, only an extremely limited number of papers can be found in literature focusing on T-joints of titanium alloys. In particular, as far as the authors know, the only group working on this topic is the one of Su et al., which published three papers during the last two years. In particular, the authors focused their attention on process feasibility for an alpha Ti alloy highlighting the main weld zones and possible defects occurring when welding two sheets as skin and one as stringer with double weld pass [13]. The same authors also compared the mechanical and microstructural properties of T joints of the same alpha Ti alloy obtained by welding two and three sheets together respectively [14]. Finally, they studied the effect of the welding parameters on the joint anisotropy in the three sheets configuration for the same alloy [15].

Numerical simulation is a fundamental tool for the considered joining by forming process design due to the complex material flow, the large number of process parameters, and the large cost which often characterizes the raw material. Due to the intricate process mechanics, simulation of the FSW process necessitates the use of a highly nonlinear numerical model. Indeed, the tool's stirring action and forward feeding cause significant deformation and distortion in the region all around the pin, resulting in heat generation through friction forces work, especially at the tool shoulder workpieces interface, and deformation one. This unique process mechanics enables the production of a solid-state weld with a smaller Heat Affected Zone (HAZ) and a dynamic recrystallized zone (RZ) close to the weld seam. Several methodologies are suitable for the numerical model of the process due to the complexity of the process. According to a review of the literature, it does not appear that there is a dominating numerical approach for simulating the process today. Using a 2D CFD technique with the commercial software FLUENT, Colegrove [16] was one of the first to investigate the influence of slip in 2D flow around the pin. The goal was to create a 2-dimensional pin profile that minimized traverse force while keeping rotating torque constant. More recently, Isa et al. [17] presented a review "Recent research advances in friction stir welding of aluminum and copper dissimilar joints," in which he discussed two different approaches: Computational Fluid Dynamics (CFD) and Coupled Eulerian-Lagrangian (CEL) Computational Solid Mechanics (CSM). Both methodologies may be used to

explore coupled frictional heat generation, the formation and growth of plastic flow regions, and three-dimensional heat and material flow, according to the scientists.

Only a few numbers of studies exist in the literature that deal with numerical models for FSW of Titanium alloys. Some of the authors [18] provided a FEM model that may predict phase transitions in Ti6Al4V titanium alloy butt joints during FSW. From the tool plunge through the final in-air cooling of the joint, the entire process was modeled using an implicit, Lagrangian, thermo-mechanically coupled with visco-plastic material characterization model. Sarikavak et al. [19] recently created a time-dependent, three-dimensional thermomechanical model of the FSW process to better understand the temperature profiles of various technical materials such as steel, aluminum alloys and titanium alloys. The maximum temperature gradients on the y- and z-axes were located at the outside diameter of the shoulder radius or at the center of the weld line, according to the theoretical predictions and experimental results presented in the paper.

In this paper, a numerical model for FSW of dual phase Ti Grade5 titanium alloy aimed at determining the phases distribution in T-joints is presented. To generate proper heat input, a tool with a double shoulder has been used to weld in "transparency" skin and stringer structures. Finally, the FEM model was validated against experimental temperature measurements and used to investigate the process mechanics and predict the distribution phases along the joint. The actual joints microstructure has been acquired to assess the effectiveness of the developed tool.

2. Experimental Process

Titanium sheets of grade5, 2 mm in thickness, were employed in the testing (main mechanical properties are shown in Table 1).

Table 1. Main mechanical properties of Ti grade5.

Work material		Ti grade5
Tensile Strength, Ultimate	[MPa]	1170
Tensile Strength, Yield	[MPa]	1100
Modulus of Elasticity	[GPa]	114
Hardness	[HV]	340

The experiments were performed using an ESAB LEGIO 3ST machine with a 2.5° tilt angle (θ) and a 2.8 mm tool plunge. A force control on the stirring head was set on the machine to guarantee constant plunge conditions along the weld. The skin and stringer sheets were cut into rectangular specimens measuring 100 x 100 mm.

The CAD of the clamping fixture used in this experiment is shown in Fig. 1: steel plates, finished on the grinding machine, were employed to provide consistent pressure distribution on the stringer.

Fig. 1 CAD of the experimental clamping fixture used

The skin was clamped atop the stringer once the latter was secured between the vertical walls. To keep the pressure constant on the skin, screw grains were utilized.

It is worth noting that, for the considered joint morphology, heat propagation on the stringer is critical to obtain joint integrity. Due to the extremely low thermal conductivity of titanium, proper heat distribution on the stringer cannot be attained only by modifying technological parameters. According

to a few studies carried out by some of the authors, a pin tool with double shoulder was utilized [20]. W25Re, characterized by a melting temperature of 3050°C and a recrystallization temperature of around 1900°C, was used to as tool material. Table 2 lists the geometrical parameters utilized.

Table 2. Geometry of the utilized tungsten-rhenium tool.

Tool material		W25Re
Shoulder diameter	[mm]	14
Secondary shoulder diameter	[mm]	7
Secondary shoulder height	[mm]	1.2
Pin major diameter	[mm]	2
Pin angle	[deg]	15
Pin height	[mm]	1.2

As process parameters are considered, the tool rotation and feed rate were set at 800 rpm and 20 mm/min, respectively, based on preliminary experimental tests.
A type K thermocouple (from -200°C to 1250°C with the special limits of error of about 1.1°C) was embedded in the skin at mid thickness, at a distance of 10 mm from the welding line, in order to acquire the temperature. Three repetitions were carried out in order to assess process stability. The specimens were prepared according to ASTM E3-11 standard procedure and etched with Kroll acid for the metallographic analysis.

3. Numerical Model setup

The numerical model was developed using the commercial software DEFORM-3D™, a lagrangian implicit code, able to carry out staggered thermo-mechanical analyses. For the mechanical analysis, a rigid-viscoplastic material model was used. The two sheets, skin and stringer, were modelled as a unique workpiece. This "single block" assumption, made to avoid numerical instabilities due to the deformable-deformable contact, has already been proved effective both for butt and lap joint configuration [18]. Fig. 2 shows the meshed workpiece, assembly, and tool.

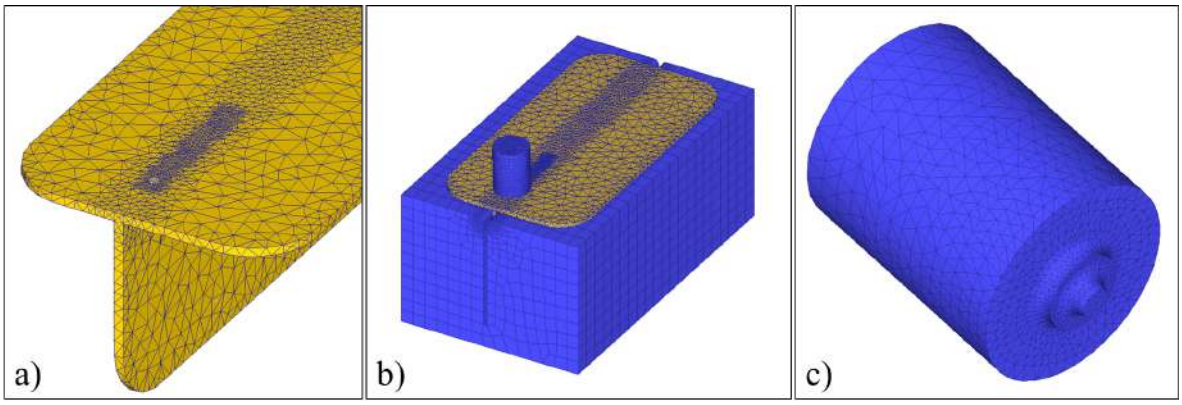

Fig. 2. The FEM model for FSW process during the plunge phase: mesh of (a) the workpiece, (b) the assembly and (c) the tool

The workpiece was meshed with about 42,000 tetrahedral elements. The entire domain was discretized with a global element size ranging from 2 mm to 6 mm and distributed using a surface curvature-aware technique. The welding line was discretized with a fixed element size of 2 mm. Because of the high gradient of deformation and temperature occurring under the tool action, a moving mesh window, with a fixed element size of 0.7 mm, was set on the welding line to follow tool feed. The Ti-6Al-4V material flow rule was characterized and validated by the some of the authors in [18]. In particular, from literature research [21] was carried out and a group of 210 plastic flow curves were collected at the varying of strain rate and temperature, starting from room temperature up to 1000 °C, 1500°C, with 50°C temperature increment between each group of curves

[22]. The curves have been implemented in the code through a tabular approach to calculate the thermo-mechanical evolutions of the considered alloy in a wide range of process conditions. Fig. 3 shows the curves obtained for strain rate of 100 1/s as a function of temperature.

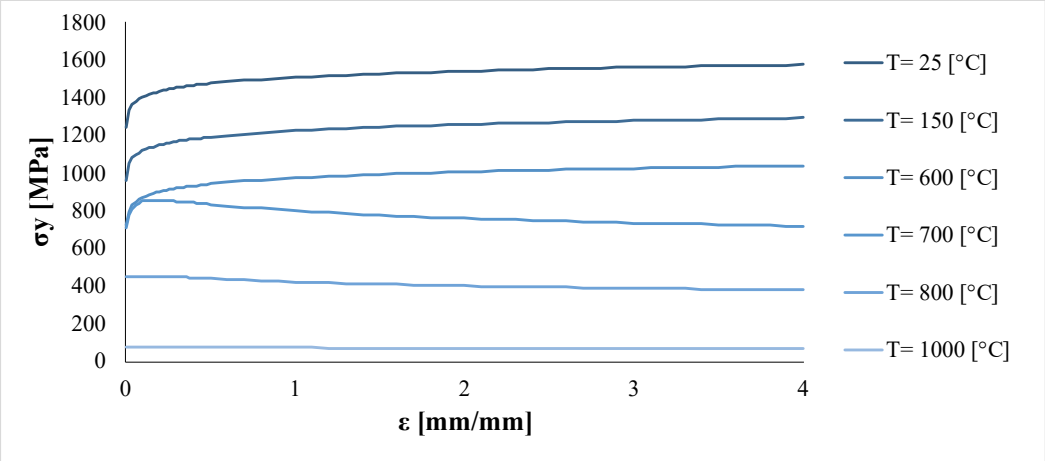

Fig. 3. Curves obtained for strain rate of 100 1/s as a function of temperature

The tool was meshed, for the thermal analysis, with about 14,000 tetrahedral elements. Constant thermal properties, namely thermal conductivity k = 59 $N/(s\,°C)$ and heat capacity c = 15 $N/(mm^2\ °C)$ were considered.

A constant interface heat exchange coefficient of 11 [N/ (mm s °C)] was utilized for the tool sheet contact surface. A constant shear friction factor of 0.6 was used for the tool-sheet interface based on a previous experimental thermal characterization and of a numerical sensitivity analysis for the shear friction factor by some of the authors [23]. For the fixture material, the DIN-C45, taken from DEFORM library, was used.

To model the transformation from the Alpha phase to the Beta one during heating up, a simplified Avrami model was utilized, as follows:

$$\theta_v = 1 - e^{\left\{-1{,}86\cdot\left[\frac{(T-T_S)}{(T_e-T_S)}\right]^{4{,}35}\right\}} \qquad (1)$$

where:

- T is the temperature.
- T_s = 600 °C is the transformation starting temperature.
- T_e = 980 °C is the end of transformation temperature.

The coefficients used in the model were calculated performing a minimization of the standard deviation between the experimental curve of the phase transformation and the numerical model curve [24]. Then to model the transformation from Beta phase to α+β one, namely the cooling stage, the TTT curves of the material were used as described in [24]. For this transformation, a diffusion model based on TTT curves was utilized:

$$\xi_{\alpha+\beta} = 1 - exp\,(-bt^n) \qquad (2)$$

Where:

- $\xi_{\alpha+\beta}$ is the transformation volume fraction
- b is the rate constant function of the temperature
- n is an empirical constant

Fig. 4 shows the utilized curve. It is worth noting that the TTT curves have been utilized instead of the more appropriate CCC curves for ease of implementation. The error introduced with this assumption can be considered acceptable as small time steps are used, and almost isothermal conditions can be considered.

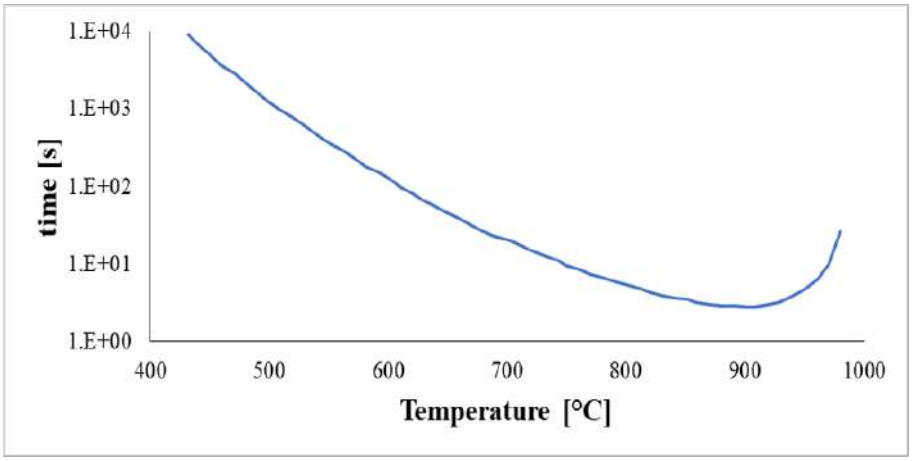

Fig. 4 TTT curve start time

The model was fine-tuned using the results of an experimental research by Malinov and Sha [25] that looked at a Ti6Al4V alloy bar with dimensions of 60x3x1.5 that was heated from room temperature to the Beta zone until the Alpha phase was almost completely transformed to the Beta phase. The workpiece was then chilled at various rates before being quenched by water and returned to room temperature. The evolution of the mixed Alpha+Beta phase was studied and reported along the process.

The experimental procedure followed in the paper was numerically modeled by the authors in [26] and the results compared.

3. Results

3.1. Experimental Results

With the aim to study the joint quality, the specimens were saw cut and the microstructure of the transverse section was analyzed.

The microstructure of the parent material is characterized by a biphasic structure (α+β) with α equiaxed grains and intergranular β-phase. In Fig. 5, a typical joint cross section obtained is shown. Furthermore, by the magnifications in two characteristic areas, the peculiar flow generating during the process by the double shoulder tool used can be seen. Two different stirring zones can be noticed in the skin and nearly the stringer respectively, due to the combination of high temperature and high strain. Furthermore, the material flow at the center of the skin results in large strain of the material, as inferred observing the vortex of material flow.

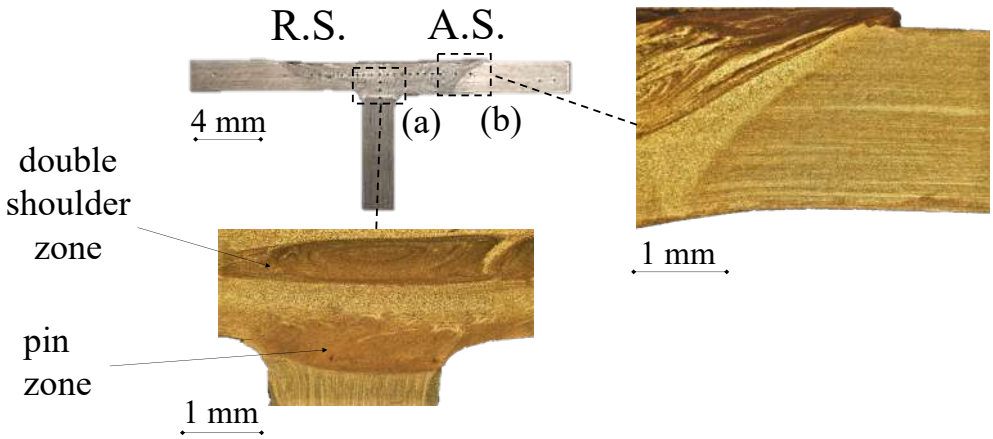

Fig. 5. Macro and micro-observations in the a) stirring zone and b) Thermo-Mechanical Affected and Heat Affected Zones for the test carried out using 800 rpm and 20 mm/min.

The presence of equiaxed α grains (bright) in a converted β-matrix (dark) can be detected in the Parent Material (Fig. 6a). However, In the Heat Affected Zone (Fig. 6b) only an increase of the grain diameters without any significant transformation due the relatively low temperature reached, i.e., lower than β-transus, can be noticed. In addition, in the Stir zone (Fig. 6d), it can be inferred that the β-transus temperature was reached as the typical lamellar α grains are observed. In the area close to the shoulder action (Fig. 6e) a large amount of alfa lamellar grains compared to alfa+ beta grains can be noticed. This effect can be due to high temperature reached and subsequent high cooling speed. The presence of the lamellar phase in the stir-zones shows that the β-transus temperature of 980 °C was reached, resulting in substantial deformations as also shown by Li et al. [27] and Rabadia et al. [4] in their studies.

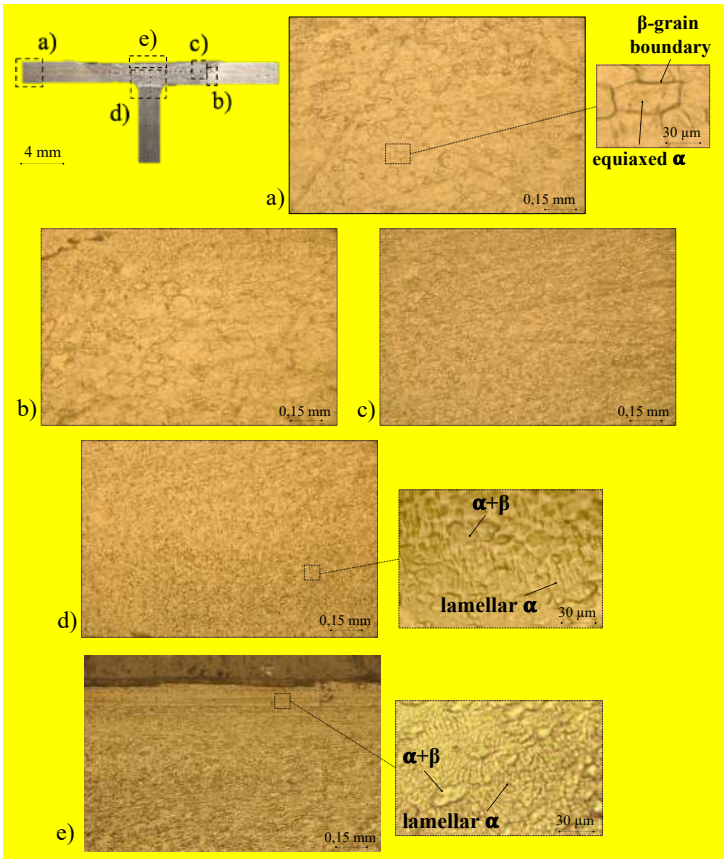

Fig. 6. Micro observations in the a) Base Material, b) Heat Affected Zone, c) Thermo-Mechanical Affected zone, d) Stir zone and e) top stir zone for the test carried out using 800 rpm and 20 mm/min.

3.2. Numerical results

3.2.1. Model validation

Because the titanium phase transformations are dominated by the workpiece thermal histories, the model was validated using the experimentally recorded temperatures. TheDEFORM-3DTM's "node tracking" function was used to determine the temperature history for a node positioned 10 mm from the welding line. After 60 mm of weld length, when the process reached a steady state, the reference transverse section was selected. Fig. 7 shows the comparison between numerically computed and empirically measured temperature. It is seen that the numerical model slightly overestimates the temperature, with a peak value of about 700°C and average error of about 3%. This difference, which was considered acceptable, can be ascribed to the heat exchange coefficient between the sheet and the fixture which will be optimized through an inverse approach in the follow up of the research activity.

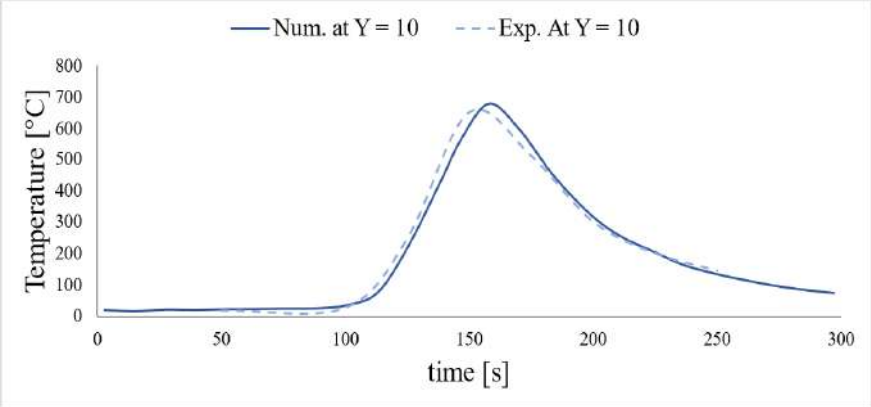

Fig. 7. Welding line distance in weld seam and 10 mm from the center

3.2.2. Field variables distribution

The second step of the developed procedure, as described in the previous paragraphs, was to simulate the welding process using a rigid-viscoplastic material model, based on the assumption that, due to the extremely large deformations that occur, elastic deformation can be ignored with no significant loss in result accuracy. This method was used to calculate nodal temperatures and their evolution throughout the FSW process. The temperature evolution on the top surface of the workpiece was represented in Fig. 8. A temperature peak of around 950 °C is attained during the tool plunge and a maximum of about 1000 °C is calculated once the process has reached its steady state.

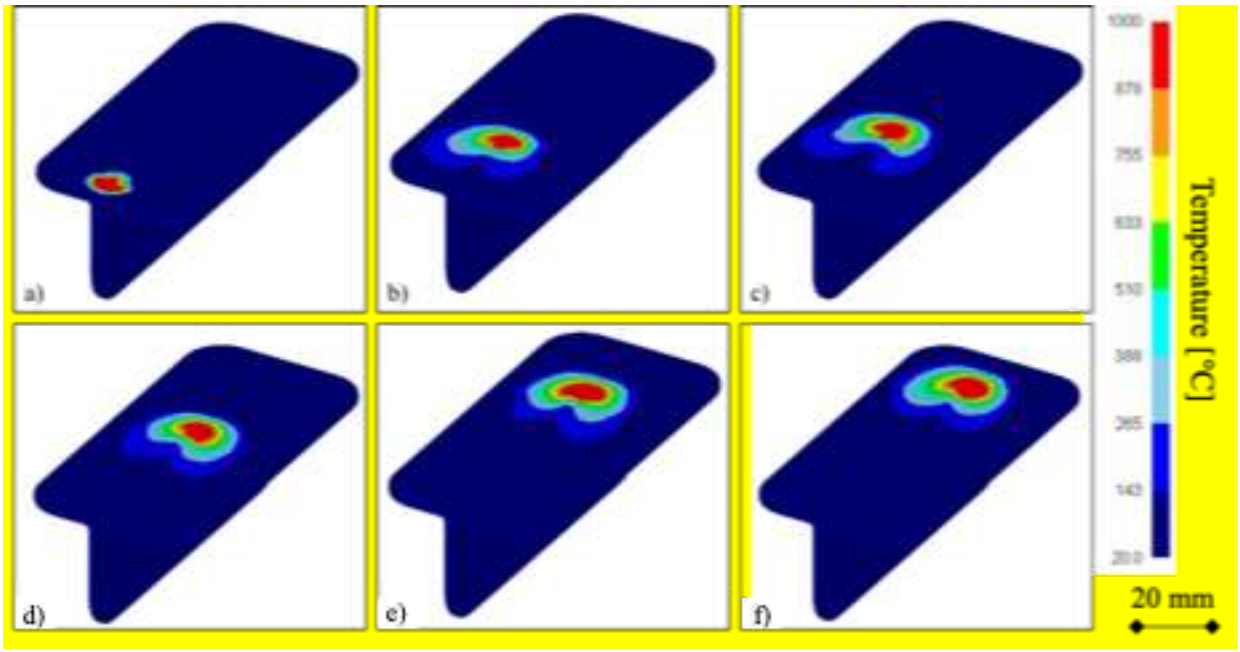

Fig. 8. Workpiece temperature evolution during the welding process simulation: (a) end of the plunge and beginning of the weld phase, (b) to (f) intermediate steps, (g) end of the process

It is observed that the "comet" shape, typical of FSW process for butt joints, presents a peculiar shape in the trailing edge of the weld, where lower temperature is obtained, for a given transverse section, in correspondence of the stringer. This is due to the considered joint morphology. In fact, due to the heat conduction in the stringer, the top surface cools down more quickly in correspondence of the weld line with respect to the other areas of the skin. This aspect can be better observed by looking at the temperature distribution in a cross section taken at mid weld length in three different times, namely when the tool axis corresponds with the transverse section, when the gap opened by the tool has just been closed, i.e., right behind the secondary shoulder, and at the end of the welding process (Fig. 9). Two observations can be made: (i) temperature distribution is non symmetric about the weld line, but it is "shifted" towards the advancing side (A.S.) of the weld. This phenomenon, known in literature for the FSW of butt joints, is amplified by the presence of the secondary shoulder, which acts as a secondary main heat source; (ii) immediately after the material closes behind the tool a higher cooling rate occurs in the welding center with respect to the one in the outer parts of the stringer. This is caused by presence of the stringer and results in the comet shape previously observed. It is worth noting that the developed model is not taking in to account the formation of martensitic phases which are likely to occur in the stir zone in the above described conditions.

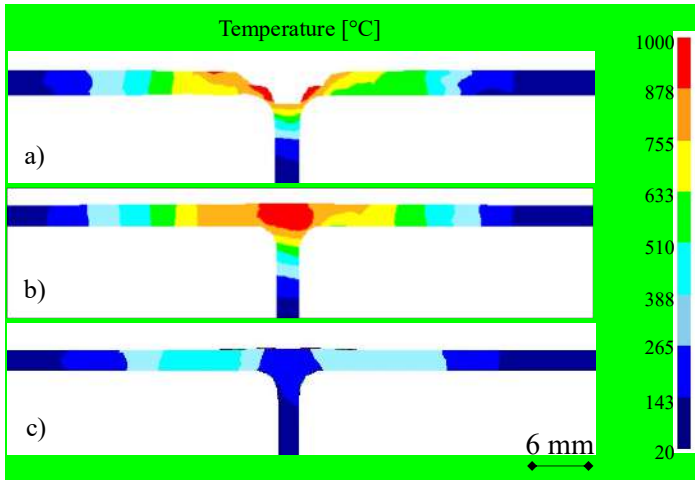

Fig. 9. Temperature distribution in a cross section at different simulation time: (a) during pass of the tool (b) immediately after the material closes behind the tool and (c) at the end of the process

In order to better understand the process mechanics, the strain distribution in the same section and time increment considered for Fig. 9b is shown in Fig. 10. As expected, extremely large values of strain are calculated due to the relatively high ratio between the tool rotation and feed rate. Additionally, a large area of the skin is involved in the high deformation area due to the secondary shoulder effect and concentrated on the advanced side (A.S.) than retreating side (R.S.) (see again Fig. 5). It is also noted that the high deformation zone involves the fillet in the A.S., while the one in the R.S. experiences less deformation. This is why, typical material flow defects (e.g. kissing bond) may occur in the R.S. fillet in FSW of T joints [28]

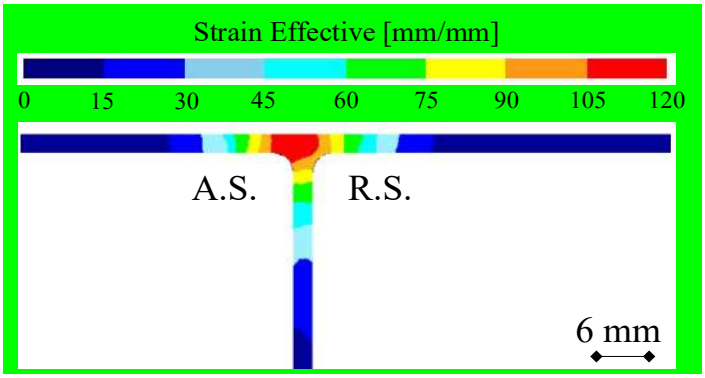

Fig. 10. Strain distribution in a cross section immediately after the material closed behind the tool

The strain rate distribution in a cross section during the tool pass confirms the highest values concentrated on the A.S. caused by the material flow induced by the combination of tool rotation and feed. Additionally, maximum strain rate is located at the edge of the secondary shoulder, thus highlighting the advantages of this tool morphology in terms of material flow – besides the already described ones in terms of heat flow - for the correct formation of the fillets.

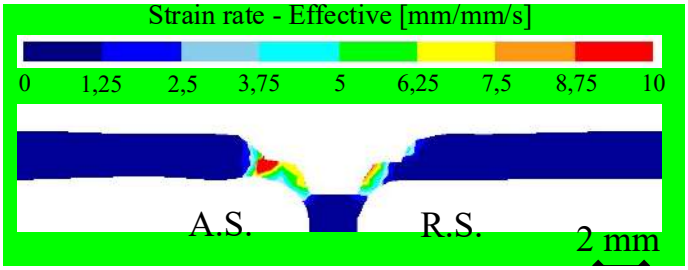

Fig. 11. Strain rate distribution in a cross section during pass of the tool

3.2.3. Phases distribution

The phase evolution was determined during and after the passage of the tool by a given cross section.

In Fig. 12 the volume fraction of the different phases during and after the transformation is presented. In particular, the α phase of the material transforms into β phase as the tool passes through. According to the considered equations, the transformation is completed only in the areas where the temperature reaches 980°C. Once the tool passage is completed, due to the temperature decrease, the β phase converts into. In this way, a final microstructure made of duplex α+β phase and α phase is obtained in the cross section. In particular, a peculiar shape, reflecting the one observed for the temperature distribution, is observed: an almost entirely α+β phase is calculated in the skin for an area characterized by a width corresponding to the one of the shoulders. Additionally, due to the lower temperatures observed in the upper part of the stringer and in the skin in correspondence of the weld line, i.e., the stringer, a concave “W” shape is observed for the final α+β phase distribution, indicating a larger volume fraction of the original untransformed α phase, consistently with the experimental observations (see again Fig. 5)

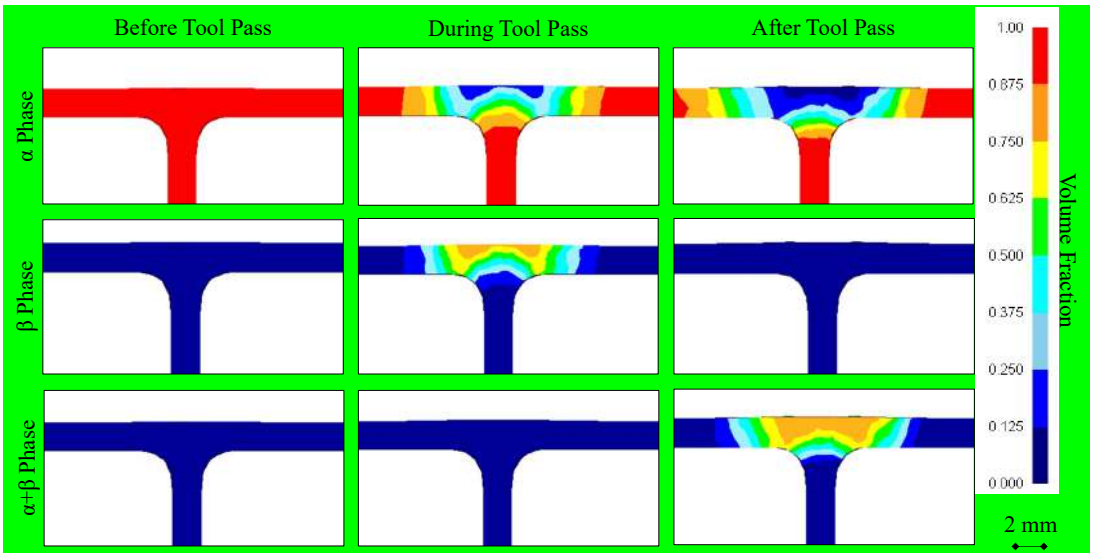

Fig. 12. Microstructure evolution caused by the tool passage

To quantitatively evaluate the above described "W" distribution, three measuring lines were considered, in a joint transverse section, at 0.5 mm, 1 mm, and 1.5 mm from the top surface of the skin (Fig. 13). From the figure it can be seen that a "U" shape is obtained close to the skin top surface, due to the more uniform temperature distribution and the lower influence of the presence of the skin. Moving towards the bottom surface of the skin, the W-shape becomes more apparent and obvious (Fig. 13c). In addition, the maximum cooling rate is obtained in the center, as is the maximum transformation of α to β, which is approximately 10% higher. Finally, as expected, the extension of the area involved by the α+β phase transformation reduces as the distance from the top increases.

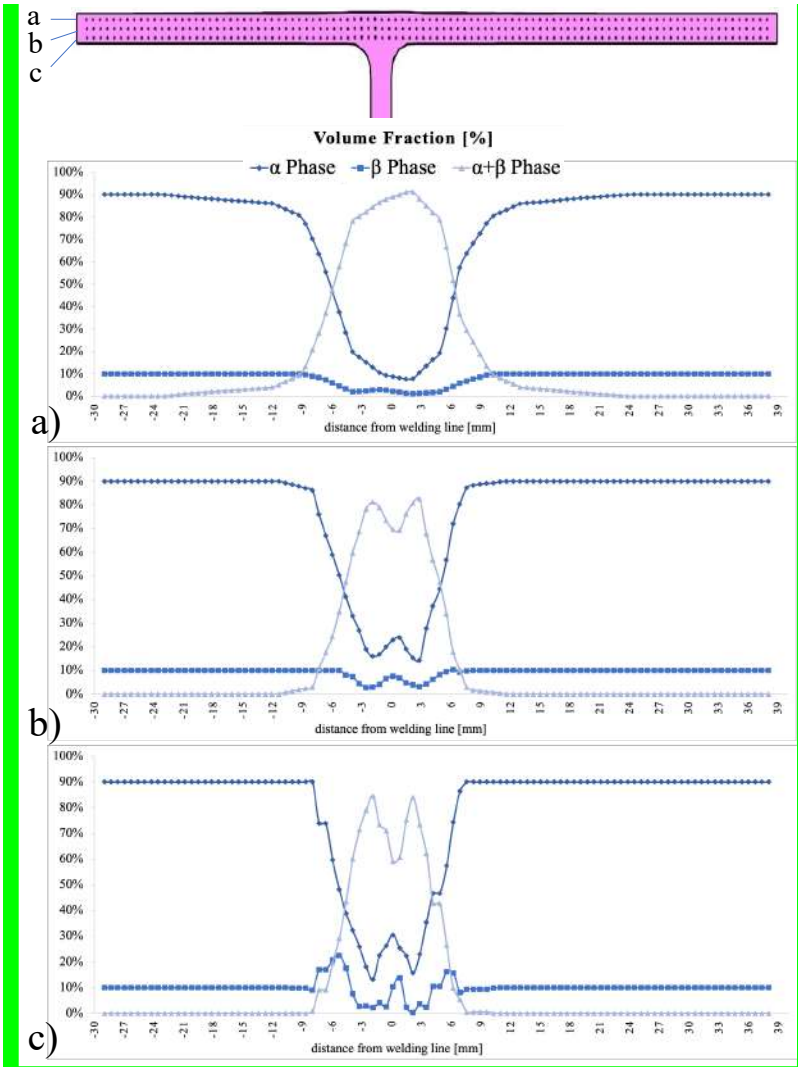

Fig. 13. α, β and α+β volume fractions at the varying of the distance from the weld center for three measurement lines at (a) 0.5 mm, (b) 1 mm and (c) 1.5 mm from the top surface

Finally, Fig. 14 depicts a bars plot of phase as a function of time at six different points equally spaced of 5 mm. The locations under consideration were in a cross section at half weld length, three at mid thickness of the skin, and three on the top of the skin. Regarding the external points (Fig. 14c and Fig. 14f), no change occurs at the farthest place from the welding center due to the low temperature reached. Transformation can be seen in the Heat Affected Zone from α in α+β structure with larger α+β volume fraction close to the top surface (Fig. 14e). The stir zone is characterized by a higher volume fraction of α+β phase with respect to α phase, (Fig. 14b and Fig. 14e). Again, due to the higher temperature obtained, the transformation into α+β close to the top surface is almost complete with respect to the one at middle thickness (Fig. 14a and Fig. 14d).

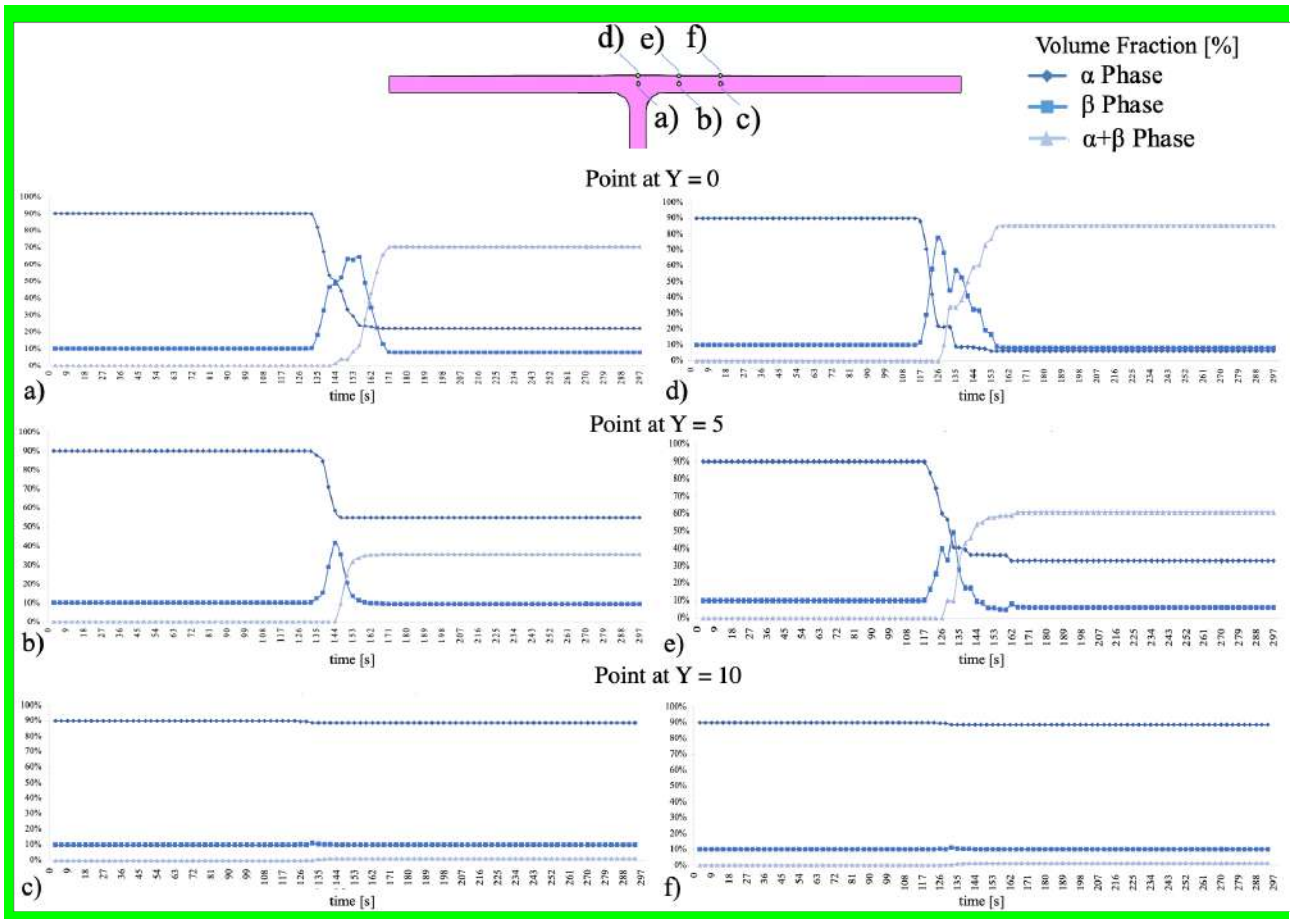

Fig. 14. Phase transformation as a function of time at different points at 0, 5 and 10 mm from the welding line

4. Summary and Conclusions

In the paper, the results of a numerical investigation focused to highlight the phase transformation occurring during FSW of Ti gr5 T-joints are presented. The entire process, from tool plunge to final in-air cool down of the joint, was modeled using an implicit, Lagrangian, thermo-mechanically coupled with viscoplastic material characterization model. The numerical model was first validated against experimental temperature, and then used to investigate the temperature and phase distributions. From the obtained results the main conclusions can be drawn:

- The temperature achieved throughout the welding operation is primarily responsible for the final microstructures, determining the presence of the β phase during welding and the subsequent formation of the α+β phase during cool down.
- Due to the use of a double shoulder tool, a large area of the skin experiences high temperature and high strain. For the considered cases study, in these areas temperatures in excess of the β transus one was obtained, resulting in the formation of duplex α+β microstructure in the final joint.
- A peculiar “W” shaped phase distribution, typical of T-joints, characterizes the central and lower part of the stir zone, as a consequence of the heat loss for conduction in the stringer. This is the result of the temperature evolution. In the upper part of the stir zone, a “U” shape is obtained, more similar to the one known for butt joints.
- The volume fraction of the duplex α+β phase is higher close to the top surface of the joints and decreases with both vertical distance and horizontal distance from the welding line. For the considered case study, a drop of about 50% is observed at a distance of 5mm from the welding line, i.e., in correspondence of the edge of the secondary shoulder, while parent material is found at a distance of 10 mm.

Future work includes the further fine-tuning of the model in terms of heat exchange coefficient determination and the application to different case studies in order to use the developed numerical tool as an effective process design tool

Acknowledgements

This study was carried out using Italian MUR funds: “on the ChOice of Manufacturing Processes for Effective Titanium componEnts (COMPETE)”, PRIN 2017.

Declarations

- Ethical Approval the Authors Disclose potential conflicts of interest; also, the research here presented does not involve either Human Participants or Animals.
- Consent to Participate: Not Applicable
- Consent to Publish: Not Applicable
- Authors Contributions:
  - Davide Campanella: Conceiving the idea, performing experimental, analysis of the results and draft writing.
  - Livan Fratini: Overall revision and research coordination.
- Funding: This study was carried out using Italian MUR funds: “on the ChOice of Manufacturing Processes for Effective Titanium componEnts (COMPETE)”, PRIN 2017.
- Competing Interests: The Authors disclose any financial and non-financial competing interests that could inappropriately influence, or be perceived to influence, this work.
- Availability of data and materials: Not Applicable

References

1. Wang L, Lu W, Qin J, et al (2009) Influence of cold deformation on martensite transformation and mechanical properties of Ti–Nb–Ta–Zr alloy. Journal of Alloys and Compounds 469:512–518. https://doi.org/10.1016/J.JALLCOM.2008.02.032
2. Liu X, Chu PK, Ding C (2004) Surface modification of titanium, titanium alloys, and related materials for biomedical applications. Materials Science and Engineering: R: Reports 47:49–121. https://doi.org/10.1016/J.MSER.2004.11.001
3. Wang X, Wang K, Shen Y, Hu K (2008) Materials Comparison of fatigue property between friction stir and TIG welds
4. Rabadia CD, Liu YJ, Jawed SF, et al (2018) Improved deformation behavior in Ti-Zr-Fe-Mn alloys comprising the C14 type Laves and β phases. Materials & Design 160:1059–1070. https://doi.org/10.1016/J.MATDES.2018.10.049
5. Lin Z, Wang L, Xue X, et al (2013) Microstructure evolution and mechanical properties of a Ti–35Nb–3Zr–2Ta biomedical alloy processed by equal channel angular pressing (ECAP). Materials Science and Engineering: C 33:4551–4561. https://doi.org/10.1016/J.MSEC.2013.07.010
6. Colegrove PA, Shercliff HR (2005) 3-Dimensional CFD modelling of flow round a threaded friction stir welding tool profile. Journal of Materials Processing Technology 169:320–327. https://doi.org/10.1016/j.jmatprotec.2005.03.015
7. Dracup BJ, Arbegast WJ Friction Stir Welding as a Rivet Replacement Technology
8. Wadeson DA, Zhou X, Thompson GE, et al (2006) Corrosion behaviour of friction stir welded AA7108 T79 aluminium alloy. Corrosion Science 48:887–897. https://doi.org/10.1016/j.corsci.2005.02.020
9. Zhang Y, Sato YS, Kokawa H, et al (2008) Stir zone microstructure of commercial purity titanium friction stir welded using pcBN tool. Materials Science and Engineering: A 488:25–30. https://doi.org/10.1016/J.MSEA.2007.10.062
10. Pasta S, Reynolds AP (2008) Residual stress effects on fatigue crack growth in a Ti-6Al-4V friction stir weld. Fatigue and Fracture of Engineering Materials and Structures. https://doi.org/10.1111/j.1460-2695.2008.01258.x
11. S.M.O. Tavares, P.C.M. Azevedo, B. Emilio, V. Richter-Trummer, M.A.V. Figueiredo PV and PMST de C (2008) Friction stir welding of T-joints in dissimilar aluminum alloys. In: Proceedings of International Mechanical Engineering Congress and Exposition. pp 265–273

12. Liu HJ, Fujii H, Maeda M, Nogi K (2003) Tensile properties and fracture locations of friction-stir-welded joints of 2017-T351 aluminum alloy. Journal of Materials Processing Technology 142:692–696. https://doi.org/10.1016/S0924-0136(03)00806-9
13. Su Y, Li W, Gao F, Vairis A (2022) Effect of FSW process on anisotropic of titanium alloy T-joint. Materials and Manufacturing Processes 37:25–33. https://doi.org/10.1080/10426914.2021.1942911
14. Su Y, Li W, Shen J, et al (2021) Comparing the local-global deformation mechanism in different friction stir welding sequences of Ti-4Al-0.005B titanium alloy T-joints. Materials Science and Engineering A 823:. https://doi.org/10.1016/J.MSEA.2021.141698
15. Su Y, Li W, Liu X, et al (2020) Strengthening mechanism of friction stir welded alpha titanium alloy specially designed T-joints. Journal of Manufacturing Processes 55:1–12. https://doi.org/10.1016/J.JMAPRO.2020.03.032
16. Colegrove PA, Shercliff HR (2013) Development of Trivex friction stir welding tool Part 1 – two-dimensional flow modelling and experimental validation. http://dx.doi.org/101179/136217104225021670 9:345–351. https://doi.org/10.1179/136217104225021670
17. Isa MSM, Moghadasi K, Ariffin MA, et al (2021) Recent research progress in friction stir welding of aluminium and copper dissimilar joint: a review. Journal of Materials Research and Technology 15:2735–2780
18. Buffa G, Ducato A, Fratini L (2013) FEM based prediction of phase transformations during Friction Stir Welding of Ti6Al4V titanium alloy. Materials Science and Engineering A 581:56–65. https://doi.org/10.1016/j.msea.2013.06.009
19. Sarikavak Y (2021) An advanced modelling to improve the prediction of thermal distribution in friction stir welding (FSW) for difficult to weld materials. Journal of the Brazilian Society of Mechanical Sciences and Engineering 43:. https://doi.org/10.1007/s40430-020-02735-2
20. Fratini L, Micari F, Squillace A, Giorleo G (2007) Experimental Characterization of FSW T-Joints of Light Alloys. Key Engineering Materials 344:751–758. https://doi.org/10.4028/WWW.SCIENTIFIC.NET/KEM.344.751
21. Semiatin SL, Glavicic MG, Shevchenko SV, et al (2009) Modeling and Simulation of Texture Evolution during the Thermomechanical Processing of Titanium Alloys. Fundamentals of Modeling for Metals Processing 536–552. https://doi.org/10.31399/ASM.HB.V22A.A0005401
22. Sente Software - JMatPro® Material Property Optimiser (MPO). https://www.sentesoftware.co.uk/jmatpro-mpo. Accessed 9 Apr 2022
23. Buffa G, Fratini L, Pasta S, Shivpuri R (2008) On the thermo-mechanical loads and the resultant residual stresses in friction stir processing operations. CIRP Annals - Manufacturing Technology 57:287–290. https://doi.org/10.1016/j.cirp.2008.03.035
24. Buffa G, Ducato A, Fratini L (2013) FEM based prediction of phase transformations during Friction Stir Welding of Ti6Al4V titanium alloy. Materials Science and Engineering: A 581:56–65. https://doi.org/10.1016/J.MSEA.2013.06.009
25. S. Malinov, P. Markovsky, W. Sha, Z. Guo (2001) Resistivity study and computer modelling of the isothermal transformation kinetics of Ti-6Al-4V and Ti-6Al-2Sn-4Zr-2Mo-0.08Si alloys. Journal of Alloys and Compounds 1–2:181–192
26. Buffa G, Ducato A, Fratini L (2013) FEM based prediction of phase transformations during Friction Stir Welding of Ti6Al4V titanium alloy. Materials Science and Engineering A 581:56–65. https://doi.org/10.1016/J.MSEA.2013.06.009
27. Zhou L, Yu M, Zhao H, et al (2019) Dissimilar friction stir welding of AA6061 and Ti6Al4V alloys: A study on microstructure and mechanical properties. Journal of Manufacturing Processes 48:119–126. https://doi.org/10.1016/J.JMAPRO.2019.09.043
28. Buffa G, Fratini L, Ingarao G, et al (2012) An optimization procedure for the friction stir welding FEM model of corner fillet joints. Steel Research International SPL. ISSUE:567–570